Acta Pharmaceutica Sinica B 2020;10(8):1414–1425

Chinese Pharmaceutical Association
Institute of Materia Medica, Chinese Academy of Medical Sciences

Acta Pharmaceutica Sinica B

www.elsevier.com/locate/apsb
www.sciencedirect.com

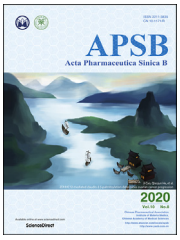

ORIGINAL ARTICLE

Discovery of the anti-angiogenesis effect of eltrombopag in breast cancer through targeting of HuR protein

Yuying Zhu[a,†], Liuqing Yang[a,†], Jiazhen Xu[a,†], Xiyan Yang[b], Pengwei Luan[b], Qianfei Cui[b], Pei Zhang[a], Feiyun Wang[a], Ruixiang Li[a], Xinyue Ding[a], Lixian Jiang[a], Guoqiang Lin[a], Jiange Zhang[a,*]

[a]*The Research Center of Chiral Drugs, Innovation Research Institute of Traditional Chinese Medicine (IRI), Shanghai University of Traditional Chinese Medicine, Shanghai 201203, China*
[b]*Institute of Drug Discovery and Development, School of Pharmaceutical Sciences, Zhengzhou University, Zhengzhou 450001, China*

Received 24 December 2019; received in revised form 4 January 2020; accepted 7 January 2020

KEY WORDS

HuR;
Eltrombopag;
Anti-tumor;
Angiogenesis;
mRNAs stability

Abstract HuR (human antigen R), an mRNA-binding protein responsible for poor prognosis in nearly all kinds of malignancies, is a potential anti-tumor target for drug development. While screening HuR inhibitors with a fluorescence polarization (FP) based high-throughput screening (HTS) system, the clinically used drug eltrombopag was identified. Activity of eltrombopag on molecular level was verified with FP, electrophoretic mobility shift assay (EMSA), simulation docking and surface plasmon resonance (SPR). Further, we showed that eltrombopag inhibited *in vitro* cell proliferation of multiple cancer cell lines and macrophages, and the *in vivo* anti-tumor activity was also demonstrated in a 4T1 tumor-bearing mouse model. The *in vivo* data showed that eltrombopag was efficient in reducing microvessels in tumor tissues. We then confirmed the HuR-dependent anti-angiogenesis effect of eltrombopag in 4T1 cells and RAW264.7 macrophages with qRT-PCR, HuR-overexpression and HuR-silencing assays, RNA stability assays, RNA immunoprecipitation and luciferase assays. Finally, we analyzed the *in vitro* anti-

Abbreviations: ARE, AU-rich element; ELB, eltrombopag; ELISA, enzyme linked immune sorbent assay; EMSA, electrophoretic mobility shift assay; FP, fluorescence polarization; HTS, high-throughput screening; HuR, human antigen R; HUVEC, human umbilical vein endothelial cell; IHC, immunohistochemistry; qRT-PCR, quantitative real-time PCR; RIP, RNA immunoprecipitation; SPR, surface plasmon resonance.

*Corresponding author. Tel./fax: +86 21 51323104.
E-mail address: jgzhang@shutcm.edu.cn (Jiange Zhang).
[†]These authors made equal contributions to this work.

Peer review under responsibility of Institute of Chinese Pharmaceutical Association and Institute of Materia Medica, Chinese Academy of Medical Sciences.

https://doi.org/10.1016/j.apsb.2020.02.007

angiogenesis effect of eltrombopag on human umbilical vein endothelial cells (HUVECs) mediated by macrophages with cell scratch assay and *in vitro* Matrigel angiogenesis assay. With these data, we revealed the HuR-dependent anti-angiogenesis effect of eltrombopag in breast tumor, suggesting that the existing drug eltrombopag may be used as an anti-cancer drug.

1. Introduction

Eltrombopag is an oral drug approved for the treatment of chronic immune thrombocytopenia[1], thrombocytopenia in patients with hepatitis C[2], and severe aplastic anemia[3] as agonist of thrombopoietin receptor (TpoR). Thrombocytopenia is also a common problem in patients with cancer, and recent studies have shown the efficiency of eltrombopag in managing thrombocytopenia associated with cancer chemotherapy[4,5]. During studies of eltrombopag in cancers, its ability to inhibit the proliferation of cancer cell lines was also reported[6−9]. However, the anti-tumor effect and mechanism of eltrombopag remain elusive. In continuation of our project exploring anticancer drugs with a high-throughput screening (HTS) system based on HuR-RNA interaction, eltrombopag was screened out. As the advantage of eltrombopag in controlling thrombocytopenia induced by cancer chemotherapy, exploring its anticancer effects and mechanisms is of great significance.

The target HuR used in our HTS system is an mRNA-binding protein that regulates the stabilization of AU-rich element (ARE)-controlled mRNAs involved in the cellular response to proliferative, apoptotic, inflammatory and immune stimuli[10]. Cumulative data have shown that elevated HuR levels are correlated with advanced clinical pathological parameters in various cancer types[11]. The ubiquitous expression of HuR in malignant clinical samples and its consistent role in tumor formation and progression make it a suitable drug target for cancer therapy. In recent years, several HuR inhibitors have been identified: dehydromutactin, okicenone and MS-444 could inhibit HuR oligomerization and disrupt HuR-targeted mRNA interaction (*Tnfα*, *Il-2*, *Cox-2*)[12]; quercetin and other flavonoids could disrupt HuR binding to *Tnfα*, *C-fos*, *Il-2* and *Cox*-2 mRNAs[13]; mitoxantrone and DHTS-I disrupt HuR binding to *Tnfα* mRNA[14]; CMLD 1-6 disrupt HuR binding to *Msi1* and *Xiap* mRNAs[15]; tanshinone and its derivatives disrupt HuR binding to *Erbb2*, *Ctnnb1* and *Vegf-a* mRNAs[16]. Among these inhibitors, MS-444[17] and DHTS-I[18] have been identified with efficient anti-tumor effect in mouse models. Thus, the employment of HuR in drug discovery still needs more efforts.

Tumor angiogenesis is one of the vital aspects for cancer development regulated by HuR, which is involved in the regulation of angiogenesis-related genes, such as *Vegf-a*, *Mmp9*, *Hif-1α* and *Cox-2*[19,20]. HuR-dependent regulation of tumor angiogenesis occurs mainly in cancer cells and tumor-associated macrophages. The proangiogenic role of HuR in macrophages has been demonstrated in macrophage-specific *Hur* knockout mice, in which microvascular angiogenesis was significantly attenuated[21,22].

In this study, we reported HuR as a new target for the clinical drug eltrombopag, and the *in vitro* anticancer effect of eltrombopag was confirmed in multiple cancer cell lines. Meanwhile, the *in vivo* inhibitory activity of eltrombopag on tumor growth and tumor angiogenesis was verified in mice bearing 4T1 cell allografts. Furthermore, the HuR-dependent molecular mechanism of eltrombopag in tumor angiogenesis was studied in detail in 4T1 cells and RAW264.7 macrophages, and the impact of eltrombopag on HUVEC phenotypes mediated by macrophages was also described. With these data, we suggest the potential of eltrombopag as a valuable anti-cancer angiogenesis drug in the clinic.

2. Materials and methods

2.1. Plasmids construction and proteins purification

The GST-HuR expression plasmid was a kind gift from Dr. Myriam Gorospe, and the HuR RRM12 (residues of 18−186) sequence was cloned into a pET30a(+) vector to produce a His6-RRM12 expression plasmid. Full-length *Hur* gene was cloned into pCMV6 vector to generate pCMV6-HuR plasmid. The 45-bp ARE sequence (5′-AAUUC UACAU ACUAA AUCUC UCUCC UUUUU UAAUU UUAAU AUUUG-3′) of *Vegf-a* mRNA ($ARE^{Vegf\text{-}a}$) was inserted into the 3′ UTR of the *Firefly* luciferase gene in the dual luciferase reporter plasmid pmirGLO (VT1439, Youbao Biotechnology, Chongqing, China) to obtain a pmirGLO-ARE plasmid (Fig. 5D).

GST-HuR and His6-RRM12 expression plasmids were transformed into *Escherichia coli* Rosetta (DE3) competent cells, and the HuR or RRM12 proteins were induced and purified as described previously[23]. Purified HuR proteins were cleaved by recombinant thrombin to remove the GST tags. Fractions of pure proteins were pooled together and concentrated by ultrafiltration before being stored at −80 °C.

2.2. Fluorescence polarization (FP) assays

5′-FAM-labeled $ARE^{Vegf\text{-}a}$ sequence was synthesized by Sangon Biotech (Shanghai, China). The HTS system based on HuR and $ARE^{Vegf\text{-}a}$ interaction was established with FP technique. For the screening, a previously described HuR inhibitor DHTS-I[18] was used as positive control, and DMSO was used as negative control. The HTS system was evaluated with Z' factor for quality control: $Z' = 1-(3\text{ SD of positive control}+3\text{ SD of negative control})/|\text{mean of positive control}-\text{mean of negative control}|$[24].

A library includes 4200 compounds were screened, and details of the compound library are shown in Supporting Information Table S1, which includes clinical drugs and derivatives. For the primary screening, the reaction includes 20 nmol/L FAM-labeled $ARE^{Vegf\text{-}a}$, 500 nmol/L full-length HuR and 100 μmol/L compound in Tris buffer (25 mmol/L Tris, pH 8.0). The reactions were incubated at room temperature for 10 min, and then detected with Multiscan Spectrum (Tecan M1000Pro, Tecan, Switzerland) at the wavelength of excitation 470 nm and emission 518 nm. Eltrombopag was selected out from the screening for further study. Dose-dependent assays of eltrombopag were carried out using the FP

method with 20 nmol/L FAM-labeled ARE$^{Vegf\text{-}a}$, 500 nmol/L full-length HuR or HuR RRM12 protein, and different concentrations of eltrombopag in Tris buffer.

2.3. Electrophoretic mobility shift assays (EMSA)

The disruption effects of eltrombopag or DHTS-I were confirmed by EMSA. The reaction system contained 20 nmol/L FAM-labeled ARE and 500 nmol/L HuR protein in the presence or absence of active compounds. The reaction was resolved by a 1% native agarose gel at 4 °C and 50 V for 50 min in 0.5 × TBE buffer as described previously with slight modification[25]. The resulting gels were visualized by fluorescence imaging using a Typhoon FLA 9500 imager (Typhoon FLA 9500, GE Healthcare, Piscataway, NJ, USA) at wavelength of 470 nm.

2.4. Molecular docking

Molecular docking was performed using the X-ray crystal structure of HuR RRM12 (PDB ID: 4ED5) in the RNA-free form[26]. Preparations of RRM12 and eltrombopag were carried out by the plugin using scripts from the AutoDock Tools package, and the binding site was defined manually according to the RNA-binding area[17]. Then, the docking run was started with AutoDock, and the interaction maps were obtained[27]. The conformation with the lowest docking energy was included in our study, and finally, the surface electrostatic potential of the model was calculated, and an image was generated with PyMol[28].

2.5. Surface plasmon resonance (SPR) assay

The interaction between eltrombopag and RRM12 domain of HuR protein was evaluated by SPR with a BIAcore T200 instrument (BIAcore T200, GE Healthcare, Chicago, IL, USA) as described[29]. Purified His-tagged RRM12 protein was immobilized on a sensor chip CM5, and a blank channel was used as negative control. Eltrombopag was serially diluted to different concentrations with PBS buffer, and flowed through the chip. The K_D value was calculated with a steady affinity state model by the BIAcore T200 analysis software.

2.6. Cell lines and cell culture

Murine mammary 4T1 carcinoma cells (ATCC® CRL-2539™), homo sapiens A549 lung carcinoma cells (ATCC® CCL-185™), homo sapiens NCI-H1299 lung carcinoma cells (ATCC® CRL-5803™) and homo sapiens SMMC7721 liver carcinoma cells were cultured in RPMI 1640 medium; murine LLC1 lung carcinoma cells (ATCC® CRL-1642™) and murine RAW264.7 macrophage cells (ATCC® TIB-71) were cultured in Dulbecco's modified Eagle's medium (DMEM); and human umbilical vein endothelial cells (HUVECs, ATCC® CRL-1730) were cultured in F-K12 medium. All media were supplemented with 10% fetal bovine serum (FBS) and 1% penicillin-streptomycin, and the cells were cultured at 37 °C in a 5% humidified CO_2 incubator. HuR over-expressing (HuROE) cells of 4T1 were obtained by transient transfection of pCMV6-HuR vector with LipoHigh liposome efficient transfection reagent (Sangon Biotech), 4T1 cells transfected with empty pCMV6 vector were used as control. Stable HuR-silenced 4T1 (ΔHuR) cells were obtained with CRISPR/Cas9-mediated knockout as described[30]. Detailed characterization and identification of the stable 4T1 ΔHuR cells were shown in Supporting Information Section 1.5. HuR protein levels of 4T1, 4T1 HuROE and 4T1 ΔHuR cells were analyzed with Western blot method (Supporting Information Fig. S6a).

For cell viability assays, MTT method was used. Cells were seeded in a 96-well tissue culture plate, incubated for 12 h, and then treated with different concentrations of eltrombopag. After 48 h of incubation, MTT solution (0.5 mg/mL) was added to the wells. The cells were then incubated for 4−5 h at 37 °C, and formazan crystals in viable cells were dissolved in 100 μL DMSO. The solubilized formazan was spectrophotometrically quantified with a Tecan M1000Pro Multiscan Spectrum (Tecan) at 490 nm.

2.7. Tumor allograft experiments

Six-week-old BALB/c mice were purchased by the Shanghai University of Traditional Chinese Medicine Institutional Animal Care and Use Committees (Shanghai, China). 4T1 cells (5×10^5) resuspended in PBS were injected into the axillary subcutaneous tissue (five mice per group). When palpable tumors (~150 mm^3) were observed, the mice received intraperitoneal (i.p.) injections of eltrombopag (75 and 150 mg/kg body weight) dissolved in PBS, gemcitabine (75 mg/kg body weight) dissolved in PBS or vehicle control every three days. The tumor volumes and body weight were measured every two days, and the tumor volumes were calculated as described previously[31]. At the termination of the experiment, the mice were euthanized, and tumors were harvested.

IHC was performed using formalin-fixed, paraffin-embedded (FFPE) tumors sectioned at a thickness of 5 μm with monoclonal anti-CD31 antibody (Abcam, Cambridge, UK), polyclonal anti-F4/80 antibody (Santa Cruz Biotechnology, Santa Cruz, CA, USA) and polyclonal anti-VEGF antibody (Santa Cruz Biotechnology). CD31, F4/80 and VEGF staining represented microvessel, macrophage and VEGF protein density, respectively. Staining and imaging were performed as described previously[32,33]. Tumor section images were analyzed with ImagePro Plus software.

2.8. Quantitative real-time PCR (qRT-PCR)

For mRNA analysis, cells were seeded in 6-well plates and treated with eltrombopag (10 μmol/L) for 12 h. Total RNA was extracted using TRIzol reagent (Sangon Biotech). For qRT-PCR assays, total RNA was used for reverse transcription with a PrimeScript™ RT reagent kit (TaKaRa, Tokyo, Japan) and with TB Green™ Premix Ex Taq™ (TaKaRa) for qRT-PCR. The mRNA levels were normalized to the β-actin mRNA level. Relative quantification was performed using the $2^{-\Delta\Delta Ct}$ method. The amplification primers were as follows: *Vegf-a* (F: 5′-TAGAG TACAT CTTCA AGCCG TC-3′, R: 5′-CTTTC TTTGG TCTGC ATTCA CA-3′), *Mmp9* (F: 5′-CGTCG TGATC CCCAC TTACT-3′, R: 5′-AACAC ACAGG GTTTG CCTTC-3′) and β-actin (F: 5′-GTCCC TCACC CTCCC AAAAG-3′, R: 5′-GCTGC CTCAA CACCT CAACC C-3′).

2.9. Western blots

Cells were seeded in 6-well plates and treated with eltrombopag (10 μmol/L) for 24 h. Cells were collected and lysed with NP40 buffer (Beyotime Biotechnology, Shanghai, China) according to the manufacturer's instructions. Protein concentrations were determined with the Enhanced BCA Protein Kit (Beyotime Biotechnology). Western blots were performed as described[34]

using antibodies (Santa Cruz Biotechnology) against VEGF-A (sc-152), MMP9 (sc-6840), HuR (sc-5261), and β-actin (sc-8432). Detections were analyzed with Azure Biosystem (Azure c600, Azure Biosystem™, Dublin, CA, USA).

2.10. RNA stability assays

4T1 and RAW264.7 cells were treated with eltrombopag (10 μmol/L) or DMSO for 12 h. Then, 40 μmol/L 5,6-dichlorobenzimidazole riboside (DRB) was added to the cells, and total RNA was extracted at five time points (0, 0.5, 1, 1.5, and 2 h) thereafter[35]. The residual levels of target mRNAs were determined by qRT-PCR and were normalized to the β-actin level. The relative amounts of the target mRNAs at time 0 before the addition of DRB were set to 100%.

2.11. Luciferase assays

Transient transfections of 4T1 cells were performed in 24-well plates using the constructed pmirGLO-ARE plasmid and LipoHigh liposome efficient transfection reagent (Sangon Biotech) in accordance with the manufacturer's instructions. After 5 h of transfection, 10 μmol/L eltrombopag or an equal amount of DMSO were added to the system, and cell lysates were tested for *Firefly* and *Renilla* luciferase activity after 24 h of incubation. The *Renilla* luciferase activity was used as a control for the transfection efficiency. Transfection with the pmirGLO plasmid was used as the blank control.

2.12. RNA immunoprecipitation (RIP)

RIP was performed as described[36] using 4T1 and RAW264.7 cells grown in 10 cm dishes and treated with 10 μmol/L eltrombopag (DMSO for control) for 12 h. The cells were lysed with polysome lysis buffer: 100 mmol/L KCl, 5 mmol/L $MgCl_2$, 10 mmol/L HEPES, pH 7.0, 0.5% Nonidet P-40, 1 mmol/L DTT, 100 U/mL RNasin RNase inhibitor (Sangon Biotech) and 2 μL/mL protease inhibitor cocktail (Sangon Biotech). Equal amounts of cytoplasmic lysates (300 μg protein) were first incubated with Protein A/G beads (Santa Cruz Biotechnology) for preclearing, and then,

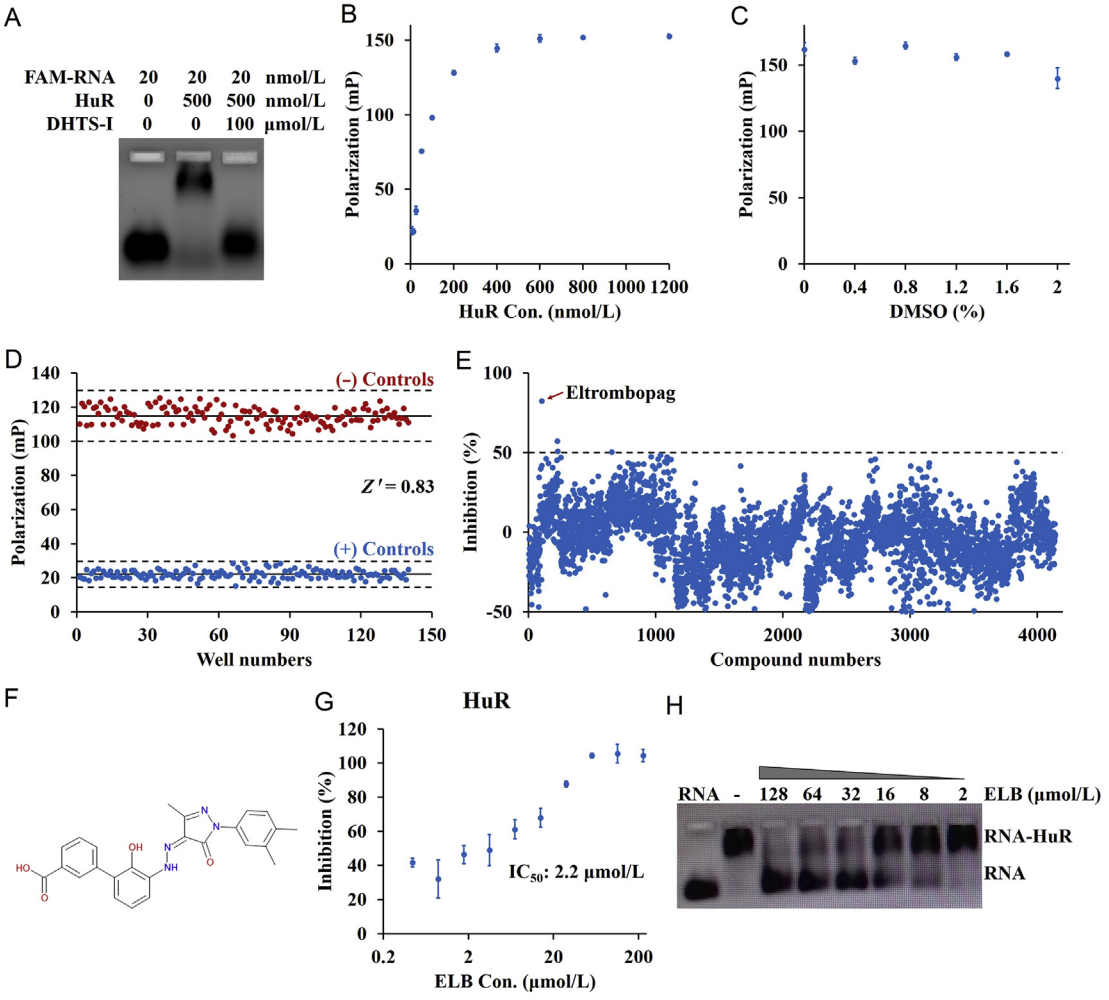

Figure 1 Identification of eltrombopag from an FP-based screening system. (A) Confirmation of the HuR-ARE$^{Vegf\text{-}a}$ interaction and disruption by the positive compound DHTS-I in EMSAs. (B) Binding assays of different concentrations of HuR protein and 20 nmol/L FAM-labeled ARE$^{Vegf\text{-}a}$ using the FP method. (C) FP assays treated with DMSO (for compound dissolution). (D) Evaluation of the established FP screening system with the Z' factor. (E) FP-based HTS of the 4200 compounds. (F) Chemical structure of eltrombopag. (G) FP-based IC_{50} assay of the effect of eltrombopag on the interaction between full-length HuR and ARE$^{Vegf\text{-}a}$. (H) EMSA showing the disruption effect of eltrombopag on the interaction between full-length HuR and ARE$^{Vegf\text{-}a}$. Data are presented as mean ± SD, $n = 3$.

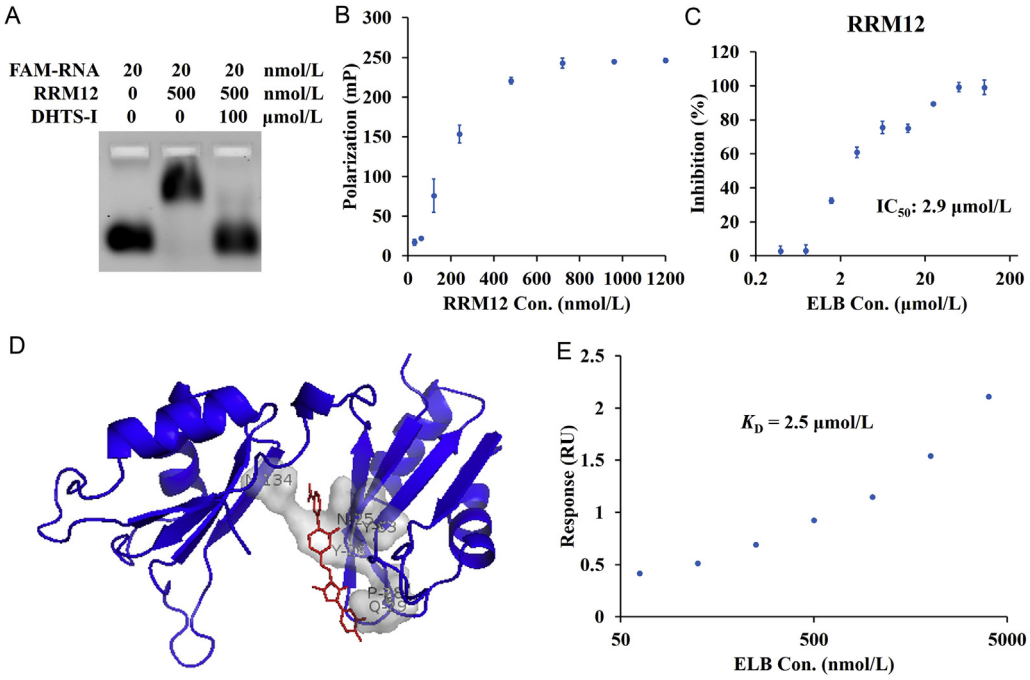

Figure 2 Eltrombopag disrupts the interaction between HuR RRM12 and ARE$^{Vegf\text{-}a}$. (A) Confirmation of the RRM12-ARE$^{Vegf\text{-}a}$ interaction and disruption by DHTS-I in EMSAs. (B) Binding assays of different concentrations of RRM12 protein and 20 nmol/L FAM-labeled ARE$^{Vegf\text{-}a}$ using FP method. (C) FP-based IC_{50} assay of the effect of eltrombopag on the interaction between the RRM12 protein and ARE$^{Vegf\text{-}a}$. (D) Computer simulation of eltrombopag binding to RRM12. (E) SPR analysis of eltrombopag binding to RRM12 protein. Data are presented as mean ± SD, $n = 3$.

Protein A/G beads coated with mouse anti-HuR or IgG antibody (Santa Cruz Biotechnology) were mixed with the lysates overnight at 4 °C. The reactions were washed with polysome lysis buffer and total RNA was isolated from the immunoprecipitates with phenol/chloroform/isoamyl alcohol. The analysis of *Vegf-a* and *Mmp9* mRNA levels was performed with qRT-PCR as described above, and fold enrichment was calculated as $2^{-\Delta\Delta Ct}$.

2.13. *Enzyme-linked immune sorbent assays (ELISA)*

The cultured RAW264.7 cells were centrifuged at 5000 rpm (Sorval Legen Micro 21R Microcentrifuge, Thermo Scientific™) for 5 min at 4 °C, and the supernatants were collected for VEGF and MMP9 detection. VEGF and MMP9 protein levels were measured by ELISA according to the manufacturer's instructions (NeoBioscience, Shanghai, China).

2.14. *Cell scratch assays*

To detect the migration capacity of HUVECs treated with supernatant from eltrombopag-treated RAW264.7 macrophages, scratch assays were performed as described previously[37]. The cell monolayers were scratched with pipet tip to create a straight line "scratch", and the cells were incubated with medium containing 50% supernatant from eltrombopag-treated (10 μmol/L) or non-eltrombopag-treated RAW264.7 macrophages for 24 h. Images were captured with a cell culture microscope (N-SIM, Nikon, Tokyo, Japan), and the scratch area was evaluated to determine the migration rates using ImageJ software (NIH, Bethesda, MD, USA). The supernatants from RAW264.7 cells were collected after incubation with 10 μmol/L eltrombopag (or DMSO) for 24 h. HUVECs were also analyzed for migration capacity impacted directly by 10 μmol/L eltrombopag with the scratch assays.

2.15. *Invitro Matrigel angiogenesis assays*

In vitro Matrigel angiogenesis assays were performed as described[38] in 24-well plates coated with Matrigel. HUVECs were incubated with medium containing 50% supernatant from eltrombopag-treated (10 μmol/L) or non-eltrombopag-treated RAW264.7 macrophages for 6 h. Tube formation was observed and captured with Nikon cell culture microscope, and the quantification of the biological activity was measured by determining the junction number, segment number and total length of tubes with ImageJ software. The direct effect of eltrombopag (10 μmol/L) on HUVECs was also detected.

2.16. *Statistical analysis*

Two-tailed Student's *t*-test was used to determine the significance of the differences in the *in vitro* and *in vivo* assay results between the control and eltrombopag treatment groups. The raw data were analyzed using GraphPad Prism 6.0 software. All values are presented as the mean ± standard deviation (SD). *P* value was taken to indicate statistical significance.

2.17. *Ethics statement*

All animal protocols and procedures were approved by the Shanghai University of Traditional Chinese Medicine Institutional

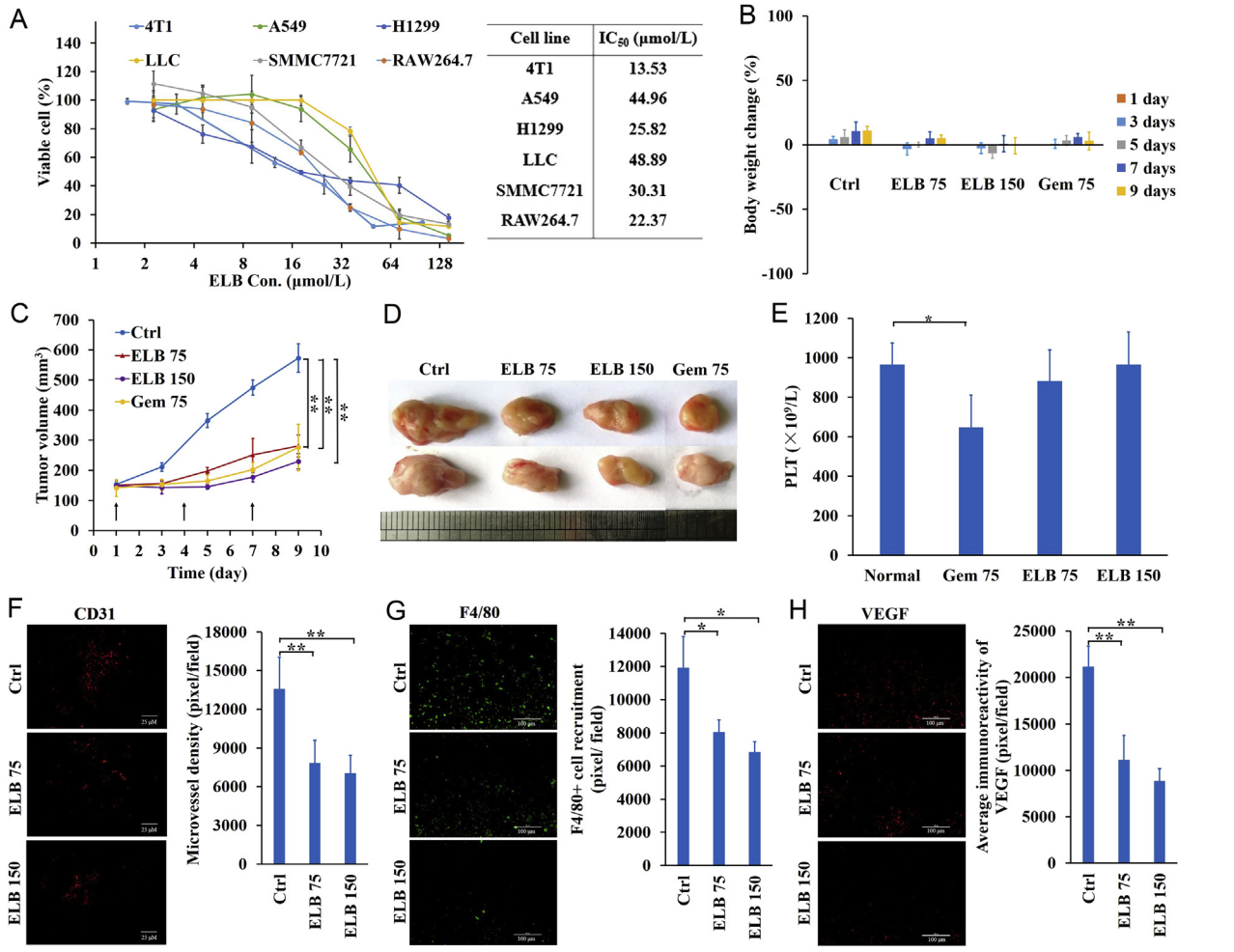

Figure 3 Anti-tumor effect of eltrombopag in tumor-related cell lines and in mice bearing 4T1 cell allografts. (A) MTT assays of eltrombopag activity in tumor-related cell lines ($n = 3$). (B) Body weight changes of tumor-bearing mice during treatment with eltrombopag ($n = 4$). (C) Tumor volume of 4T1 cell implants in mice treated with eltrombopag, gemcitabine or vehicle ($n = 4$). (D) Representative tumors excised at day nine are shown. (E) Platelet levels of mice ($n = 3$). Normal represents mice with no tumor. (F) 4T1 allograft tumors were analyzed for microvessel density using anti-CD31 antibody ($n = 3$). (G) IHC detection of F4/80 (representative of macrophages) in 4T1 tumors ($n = 3$). (H) IHC detection of VEGF in 4T1 tumors ($n = 3$). Gem, gemcitabine. Data are presented as mean ± SD; *$P < 0.05$. **$P < 0.01$.

Animal Care and Use Committees and were carried out in accordance with the guidelines outlined in the Guide for the Care and Use of Laboratory Animals published by National Institute of Health. All experiments were carried out in compliance with ARRIVE guidelines[39].

3. Results

3.1. *Identification of eltrombopag from an HTS system based on HuR-ARE$^{Vegf\text{-}a}$ interaction*

We established an *in vitro* FP-based screening system for potential inhibitors of HuR-ARE$^{Vegf\text{-}a}$ interaction. The affinity activity of purified HuR protein and the synthetic FAM-labeled ARE$^{Vegf\text{-}a}$ was confirmed *via* EMSA analysis (Fig. 1A). To optimize the concentration of HuR protein used in the FP assays, 20 nmol/L labeled ARE$^{Vegf\text{-}a}$ and different concentrations of HuR protein were added to each reaction, and FP assays were performed. As shown in Fig. 1B, the FP value reached a plateau when 500 nmol/L of HuR was added to the reaction. In addition, no obvious impact to FP values was found within 2% DMSO (*v*/*v*) (Fig. 1C). Finally, to determine the well-to-well variation in FP-based binding assays, 40 negative controls (1%, *v*/*v*, of DMSO only) and 40 positive controls (100 μmol/L DHTS-I) were evaluated, resulting in a Z' factor of 0.83 (>0.5) (Fig. 1D), which is considered acceptable for the HTS system.

With the established HTS system, a primary screening was performed for a set of 4200 compounds, among which eltrombopag (Fig. 1F) was a positive hit (Fig. 1E). FP assays shown IC_{50} of eltrombopag was 2.2 μmol/L (Fig. 1G). The activity was also supported by EMSA results (Fig. 1H), which also indicate that eltrombopag could block the binding of RNA to HuR protein.

3.2. *Eltrombopag binds HuR RRM12 by competing with ARE$^{Vegf\text{-}a}$*

As RRM12 is the main ARE-binding domain of HuR protein, we further expressed and purified RRM12 protein. We first confirmed the binding activity of RRM12 and ARE$^{Vegf\text{-}a}$ sequence *via* EMSA

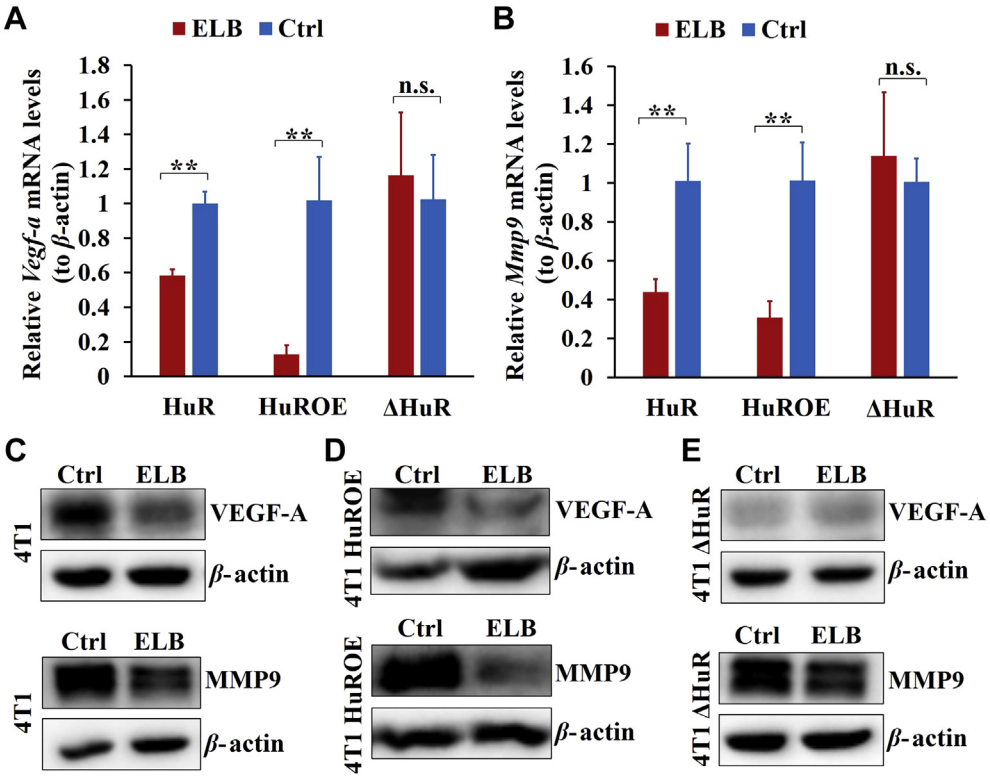

Figure 4 Eltrombopag's effect in 4T1, 4T1 HuROE and 4T1 ΔHuR cells. (A) and (B) qRT-PCR showing relative mRNA amounts of *Vegf-a* and *Mmp9* in 4T1, 4T1 HuROE and 4T1 ΔHuR cells after exposure to 10 μmol/L eltrombopag for 12 h, normalized to β-actin mRNA levels. (C) VEGF-A and MMP9 protein levels impacted by 10 μmol/L eltrombopag in 4T1 cells. (D) VEGF-A and MMP9 protein levels impacted by 10 μmol/L eltrombopag in 4T1 HuROE cells. (E) VEGF-A and MMP9 protein levels impacted by 10 μmol/L eltrombopag in 4T1 ΔHuR cells. Data are presented as mean ± SD, $n = 3$; $^{**}P < 0.01$. n.s., no significant difference.

(Fig. 2A), and 500 nmol/L optimized RRM12 protein (Fig. 2B) was used for FP detection. The IC_{50} value for eltrombopag to disrrupt RRM12-ARE$^{Vegf\text{-}a}$ interaction was determined using the FP assays to 2.9 μmol/L (Fig. 2C), which is similar to that of HuR-ARE$^{Vegf\text{-}a}$ interaction, and indicates the possibility that RRM12 contains the site at which eltrombopag acts. Thus, we then simulated the interaction mode of eltrombopag and RRM12 using AutoDock4.2.6. As shown in Fig. 2D, the eltrombopag molecule could bind through hydrogen bond interactions to the positively charged cleft formed by the two RRM domains, which is also the binding position of U-rich RNA[26]. We also detected the interaction between eltrombopag and RRM12 protein with SPR assay. The result shows that eltrombopag was able to bind to RRM12 protein with a K_D value of 2.5 μmol/L (Fig. 2E). These data show that eltrombopag could block the binding of HuR to RNA by targeting the HuR RRM12 domain.

3.3. *Eltrombopag exhibits anti-tumor effects in vitro and in vivo*

We firstly detected eltrombopag's cell toxicity to five cancer cell lines and one macrophage cell line: 4T1, A549, H1299, LLC, SMMC7721 and RAW264.7. As shown in Fig. 3A, eltrombopag could inhibit the *in vitro* cell viability of all the detected cell lines. As eltrombopag was most effective to 4T1 cells, we selected 4T1 cells for further *in vivo* anti-tumor and mechanistic analyses. Meanwhile, macrophages are crucial drivers of tumor progression, especially tumor angiogenesis, thus the macrophage-mediated anti-tumor mechanism of eltrombopag is also discussed below.

To detect the *in vivo* anti-tumor effect of eltrombopag, we established mice bearing allografts with 4T1 cell lines. Over the course of the experiment, eltrombopag was well tolerated, and no signs of acute toxicity were observed (Fig. 3B and Supporting Information Fig. S2). Obvious anti-tumor effects of eltrombopag were observed for the 75 mg/kg dose ($P < 0.01$) and 150 mg/kg dose ($P < 0.01$) (Fig. 3C and D). A clinical used chemotherapy drug gemcitabine (75 mg/kg) was used as positive control, which showed similar anti-tumor effect to eltrombopag. As eltrombopag is a drug used for thrombocytopenia, we thus detected blood platelet levels in tumor-bearing mice treated with eltrombopag (Fig. 3E), and normal blood platelet levels were obtained, while a significant decrease was observed in tumor-bearing mice treated with gemcitabine.

The anti-angiogenesis effect of eltrombopag in 4T1 tumor tissue was surveyed. Microvessels were stained with anti-CD31 antibody, which revealed that eltrombopag treatment highly decreased the microvessel density in tumor tissues ($P < 0.01$, Fig. 3F). The tumor sections were also immunostained for macrophages, as illustrated in Fig. 3G, the macrophage number in tumor tissues was dramatically decreased in the eltrombopag-treated groups ($P < 0.05$). Meanwhile, IHC analysis indicated dramatically reduced VEGF protein levels in eltrombopag-treated tumor tissue ($P < 0.01$, Fig. 3H). The anti-angiogenesis effect of eltrombopag was also demonstrated in zebrafish model (Supporting Information Fig. S3) and polyvinyl alcohol (PVA) sponge implantation mouse model (Supporting Information Fig. S4). Collectively, eltrombopag inhibited tumor growth and

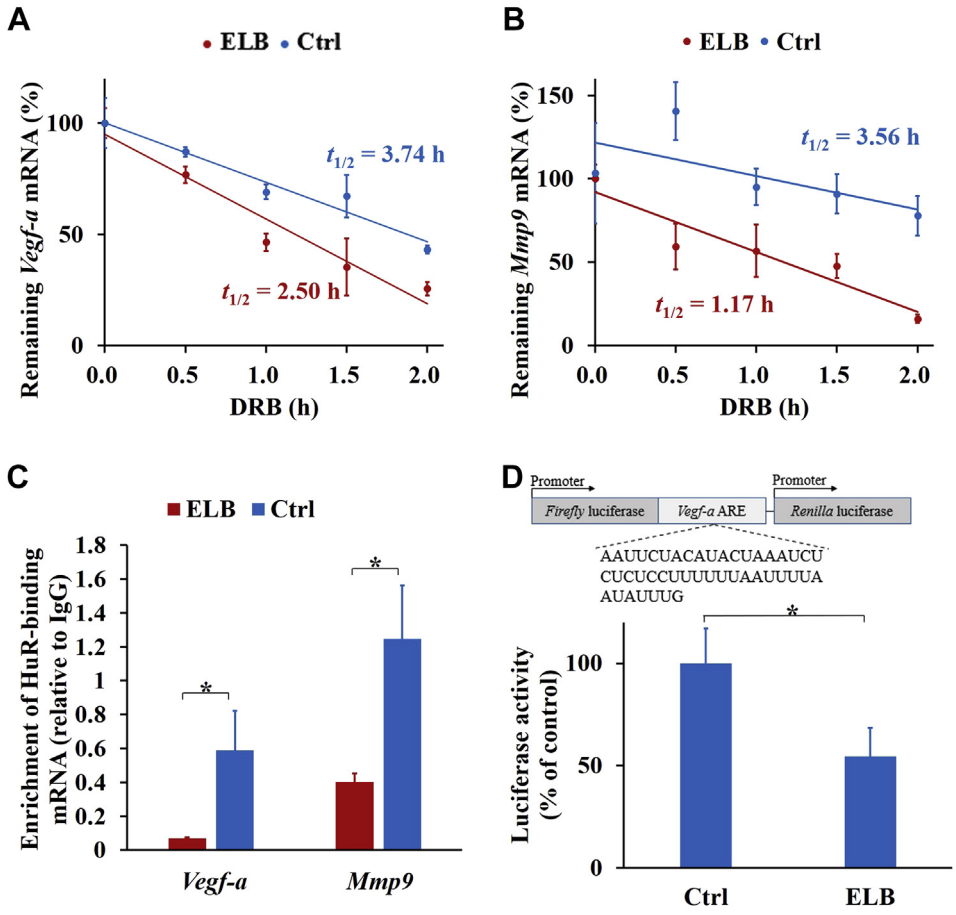

Figure 5 Impact of HuR functions by eltrombopag in 4T1 cells. (A) and (B) represented mRNA stabilization of *Vegf-a* and *Mmp9* impacted by eltrombopag respectively. (C) RIP analysis of HuR-bound mRNA (*Vegf-a* and *Mmp9*) affected by eltrombopag. IgG antibody was used as negative control of HuR antibody. (D) Luciferase activity of 4T1 cells transfected with $ARE^{Vegf\text{-}a}$-containing plasmid and treated with eltrombopag for 24 h. The *Firefly* luciferase activity was normalized to *Renilla* luciferase. Data are presented as mean ± SD, $n = 3$; $^*P < 0.05$.

angiogenesis *in vivo*, and macrophages might have an important role in the effect of eltrombopag.

3.4. *Eltrombopag regulates tumor angiogenesis-related genes in 4T1 cells through HuR-dependent mechanism*

To investigated whether the *in vitro* and *in vivo* anti-tumor effect of eltrombopag is due to targeting of HuR protein, we constructed 4T1 HuROE clone and 4T1 ΔHuR clone. The mRNA and protein levels of *Vegf-a* and *Mmp9* genes were detected respectively in 4T1, 4T1 HuROE and 4T1 ΔHuR cells. As shown in Fig. 4A and B, eltrombopag could greatly reduce mRNA amount of *Vegf-a* and *Mmp9* in both 4T1 cells ($P < 0.01$) and 4T1 HuROE cells ($P < 0.01$), while no significant change of mRNAs amounts was observed in 4T1 ΔHuR cells. Similar changes were observed for the protein levels, VEGF-A and MMP9 protein levels were dramatically decreased by eltrombopag in wild type 4T1 cells (Fig. 4C) and 4T1 HuROE cells (Fig. 4D), while in 4T1 ΔHuR cells the effect was disappeared (Fig. 4E).

For further confirmation, we also detected the mRNAs stability of *Vegf-a* and *Mmp9* gene impacted by eltrombopag in 4T1 cells, which all shown obvious reduced by eltrombopag (Fig. 5A and B). Correspondingly, to test whether the reduced mRNA stabilization induced by eltrombopag was mediated by HuR, RIP analysis was performed. The results revealed that eltrombopag reduced the number of *Vegf-a* ($P < 0.05$) and *Mmp9* ($P < 0.05$) mRNA copies selectively bound by HuR in 4T1 cells (Fig. 5C). In addition, with a dual luciferase reporter system (Fig. 5D), we found that the *Firefly* luciferase (with ARE sequence at the 3′ end) activity was dramatically decreased by eltrombopag ($P < 0.05$, Fig. 5D). With these results, we confirmed the mechanism that eltrombopag regulates angiogenesis-related mRNA levels by targeting HuR protein and reduce its binding to mRNAs in 4T1 cells.

3.5. *Eltrombopag regulates macrophage-mediated angiogenesis in HuR-dependent manner*

Macrophages play a critical role in HuR-dependent regulation of tumor angiogenesis, and thus, we also explored the HuR-dependent mechanism of eltrombopag in RAW264.7 cells. As shown in Fig. 6A, *Vegf-a* ($P < 0.01$) and *Mmp9* ($P < 0.05$) mRNA expression was downregulated by eltrombopag. In addition, VEGF and MMP9 proteins released by RAW264.7 cells were also reduced by eltrombopag (Fig. 6B and C). Furthermore, the stability of their mRNAs was significantly reduced when cells were incubated with eltrombopag (Fig. 6D and E). With RIP assays, we

confirmed that the amount of *Vegf-a* and *Mmp9* mRNAs pulled by HuR was also obviously reduced by eltrombopag (Fig. 6F).

We then investigated if the HuR-dependent mRNA decay induced by eltrombopag in RAW264.7 macrophages could affect the functions of downstream vascular endothelial cells (HUVECs). HUVECs were incubated with supernatants from eltrombopag-treated RAW264.7 (s-ELB) or non-eltrombopag-treated RAW264.7 (s-Ctrl) macrophages, and HUVEC cell viability, migration and tube formation were measured. When incubated with supernatant from eltrombopag-treated RAW264.7 macrophages, the cell viability of HUVECs was significantly inhibited (Supporting Information Fig. S7a). However, eltrombopag had no obvious effect on HUVEC viability (Fig. S7b). Next, HUVEC migration was examined with *in vitro* scratch assays. Compared with the 38.7% migration rate in the s-Ctrl group, the migration rate in the s-ELB group (14.7%) was dramatically reduced (Fig. 7A). Subsequently, using a Matrigel matrix, we found that tube formation was inhibited by supernatant of ELB-treated RAW264.7 (Fig. 7B). In contrast, HUVEC migration and tube formation were unaffected when cells were directly incubated with eltrombopag (Fig. 7C and D). These results indicate that the angiogenesis functions of HUVECs are impacted by eltrombopag through a macrophage-mediated manner.

4. Discussion

The RNA-binding protein HuR is a widely studied regulator of eukaryotic posttranscriptional gene expression that binds to AREs of mRNAs and shuttles from the nucleus to the cytoplasm to regulate the half-life and/or translation of cargo mRNAs[40]. Elevated HuR expression levels or increased cytoplasmic HuR levels have been correlated with advanced clinicopathological parameters and altered protein expression levels in malignancy, which makes HuR a putative drug target for cancer therapy[11]. In recent years, a series of HuR inhibitors have been designed for cancer therapy, including not only drugs that directly inhibit HuR translocation[41] but also inhibitors of the ARE-binding function of HuR. The existing inhibitors mainly disrupt HuR binding to tumor-promoting genes, including *Tnf-α*, *Cox-2*, *Il-1β*, *Il-2*, etc.[12,42,43]; however, HuR inhibitors to regulate tumor angiogenesis have rarely been studied. As HuR protein plays a critical role in the stability of pro-angiogenesis cytokine mRNA in different cancers[44], we established an HTS system based on the interaction of HuR and the ARE of *Vegf-a*, a widely studied pro-angiogenesis cytokine[45]. From the screening system, a positive hit eltrombopag was identified, with an IC_{50} of 2.2 μmol/L to HuR-ARE$^{Vegf\text{-}a}$ interaction. As for other HuR inhibitors, DHTS-I possesses the best activity, with an IC_{50} of 149 nmol/L for REMSA assay[42]; MS-444 with an IC_{50} of approximately 10 μmol/L for FP assay[12], and CMLD-2 with an IC_{50} of 2.4 μmol/L for FP assay[15].

Our data showed that eltrombopag is effective in disrupting the interaction between HuR protein and ARE sequence of *Vegf-a* mRNA (Fig. 1G). Structurally, HuR contains three RNA recognition motifs (RRM1, RRM2 and RRM3) and a specific nuclear-cytoplasmic shuttling sequence (HNS) between RRM2

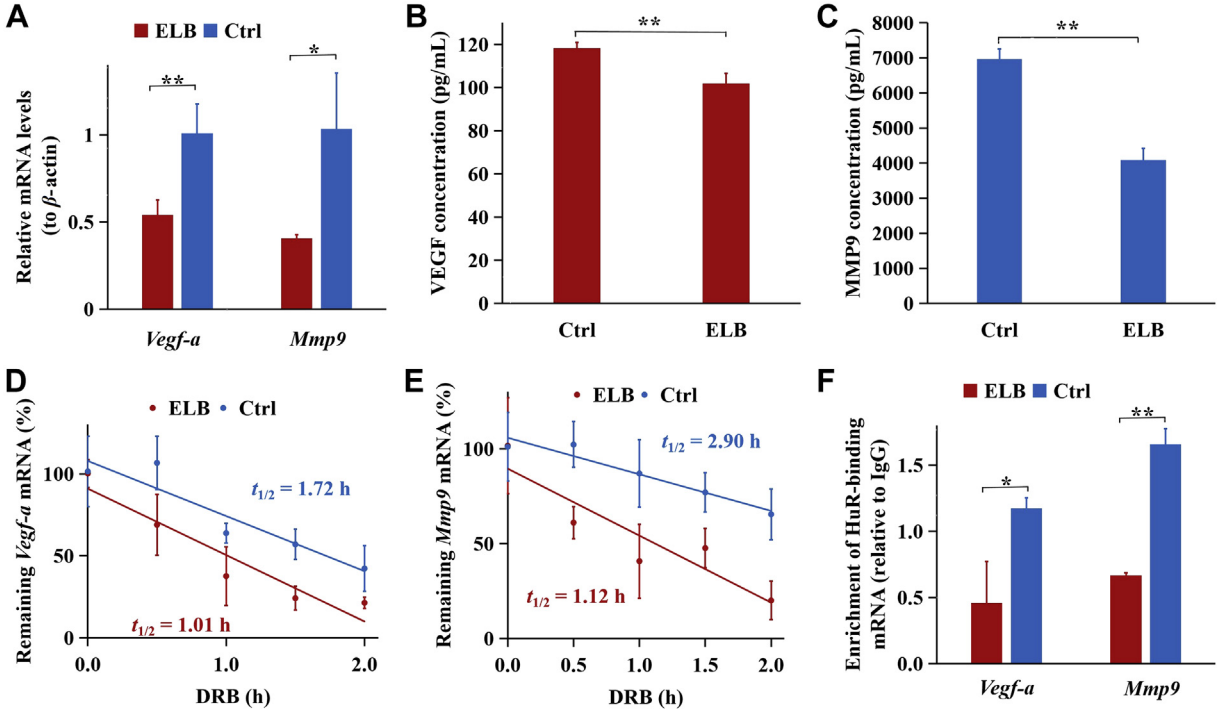

Figure 6 Eltrombopag regulated angiogenesis-related genes in RAW264.7 with HuR-dependent manner. (A) Relative *Vegf-a* and *Mmp9* mRNA levels in RAW264.7 cells after exposure to 10 μmol/L eltrombopag for 12 h, normalized to *β*-actin mRNA levels. (B) and (C) VEGF-A and MMP9 proteins released by RAW264.7 cells after exposure to 10 μmol/L eltrombopag for 24 h. ELISA assays were used for the detection. (D) and (E) present stabilization of *Vegf-a* and *Mmp9* mRNA in RAW264.7 cells affected by 10 μmol/L eltrombopag. (F) RIP analysis of HuR-bound mRNAs (*Vegf-a* and *Mmp9*) affected by 10 μmol/L eltrombopag. Data are presented as mean ± SD, $n = 3$; $^*P < 0.05$, $^{**}P < 0.01$.

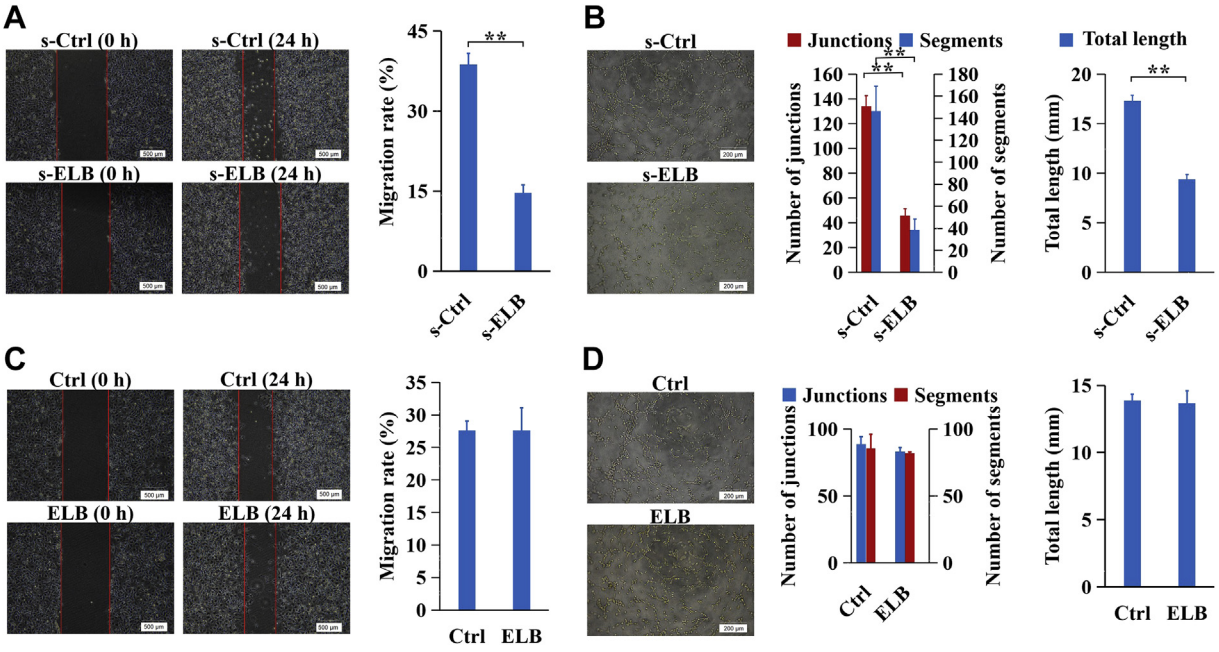

Figure 7 Functional impacts to HUVEC cells by supernatant of eltrombopag-treated RAW264.7 cells. (A) HUVEC migration affected by the supernatant from eltrombopag-treated RAW264.7 cells ($n = 3$). (B) HUVEC tube formation affected by the supernatant from eltrombopag-treated RAW264.7 cells ($n = 4$). (C) HUVEC cells migration impacted by eltrombopag directly ($n = 3$). (D) HUVEC tube formation impacted by eltrombopag directly ($n = 4$). Data are presented as mean ± SD; $^{**}P < 0.01$.

and RRM3. RRM1 and RRM2 are the most widely studied domains and contain the main ARE-binding region by forming a positively charged cleft for RNA binding[26,46]. We measured the effect of eltrombopag on the RRM12 protein and ARE interaction with FP and EMSA assays, which revealed RRM12 might be the main target region of eltrombopag. Then, with computer-aided drug modeling and SPR analysis, we found that eltrombopag likely binds directly to the positively charged cleft of HuR RRM12, implying competitive binding activity with the ARE sequence.

We also detected the *in vitro* tumor-inhibiting activity of eltrombopag, which exhibited a wide spectrum of cell toxicity in multiple cancer cell lines but no visible toxicity toward normal HUVECs, which is also supported by previous studies[6,7]. Next, we confirmed the *in vivo* anti-tumor effect of eltrombopag in 4T1 tumor-bearing mice, from which we observed obvious anti-angiogenesis activity of eltrombopag. The tumor angiogenesis involves not only cancer cells but also various tumor-associated leukocytes and stromal cells, among which macrophages are representative[47]. Thus, in this study, we explored the HuR-dependent anti-angiogenesis effect of eltrombopag in both the 4T1 cancer cell line and the RAW264.7 macrophage line. Two HuR-targeted mRNAs closely related with tumor angiogenesis, *Vegf-a* and *Mmp9*[48,49], were used to investigate the effect of eltrombopag on mRNA decay, and the half-lives of mRNAs of the two genes were found to be dramatically declined in both 4T1 and RAW264.7 cells by eltrombopag (Figs. 5 and 6). Other experiments, including RIP, luciferase assays and knockdown of HuR, demonstrated that eltrombopag affects 4T1 and RAW264.7 cells by targeting HuR protein, which is consistent with our molecular experiments.

To confirm that the anti-angiogenesis effect of eltrombopag was not through direct action on endothelial cells[50], an *in vitro* simulation test was designed in which HUVECs were incubated with supernatants from eltrombopag-treated RAW264.7 cells, and the results showed that HUVEC cell viability, migration and tube formation were all dramatically altered. However, we did not observe a direct effect of eltrombopag on HUVECs, in which HuR expression is not elevated. These results support our view that HuR inhibitors could exert effects through macrophages, which has not been discussed previously. In addition, our study confirmed that HuR might be a useful anti-angiogenesis target for tumor treatment, and this finding emphasizes the importance of HuR in the anti-cancer drug screening field.

5. Conclusions

We elucidated the anti-tumor effect and new mechanism of the clinical drug eltrombopag, where eltrombopag exhibited anti-angiogenesis effect through targeting HuR in cancer cells and macrophages. With these results, we not only find out new protein target of eltrombopag, we also exhibit the possible anti-angiogenesis mechanism in cancer mediated by macrophages. More importantly, this study further emphasizes the efficiency of HuR inhibitors for tumor inhibition, especially angiogenesis inhibition, which also promote us to develop new anti-cancer drugs based on molecular structure of eltrombopag.

Acknowledgments

We thank Dr. Myriam Gorospe for providing the GST-HuR plasmid. This work was supported by National Natural Science

Foundation of China (81573579), the New Interdisciplinary Subject Funding Program for Shanghai Traditional Chinese Medicine (E2-F18003, China), Shanghai Municipal Education Commission (SMEC, 2019-01-07-00-10-E00072, China), Science and Technology Commission of Shanghai Municipality (STCSM, 18401933500, China), Postdoctoral Science Foundation of China (A2-X1802408) and Shanghai Municipal Commission of Health and Family Planning (2018YQ003, China).

Author contributions

Yuying Zhu: conceptualization, original draft, methodology, and funding acquisition; Liuqing Yang and Jiazhen Xu: methodology and formal analysis; Xiyan Yang: investigation; Pengwei Luan and Qianfei Cui: formal analysis; Pei Zhang, Feiyun Wang and Ruixiang Li: data curation; Xinyue Ding: resources; Lixian Jiang: software; Guoqiang Lin: review and editing; Jiange Zhang: review and editing, funding acquisition and supervision.

Conflicts of interest

The authors declare that they have no competing interests.

Appendix A. Supporting information

Supporting data to this article can be found online at https://doi.org/10.1016/j.apsb.2020.02.007.

References

1. Stasi R. Eltrombopag: the discovery of a second generation thrombopoietin-receptor agonist. *Expet Opin Drug Discov* 2009;**4**:85−93.
2. Mchutchison JG, Dusheiko G, Shiffman ML, Rodrigueztorres M, Sigal SH, Bourliere M, et al. Eltrombopag for thrombocytopenia in patients with cirrhosis associated with Hepatitis C. *N Engl J Med* 2007;**357**:2227−36.
3. Gill H, Wong RSM, Kwong Y. From chronic immune thrombocytopenia to severe aplastic anemia: recent insights into the evolution of eltrombopag. *Ther Adv Hematol* 2017;**100**:159−74.
4. Hayes S, Mudd PN, Ouellet D, Johnson BM, Williams D, Gibiansky E. Population PK/PD modeling of eltrombopag in subjects with advanced solid tumors with chemotherapy-induced thrombocytopenia. *Cancer Chemother Pharmacol* 2013;**71**:1507−20.
5. Chawla SP, Staddon AP, Hendifar AE, Messam C, Patwardhan R, Kamel YM. Results of a phase I dose escalation study of eltrombopag in patients with advanced soft tissue sarcoma receiving doxorubicin and ifosfamide. *BMC Canc* 2013;**13**:121.
6. Ericksonmiller CL, Kirchner J, Aivado M, May RD, Payne P, Chadderton A. Reduced proliferation of non-megakaryocytic acute myelogenous leukemia and other leukemia and lymphoma cell lines in response to eltrombopag. *Leuk Res* 2010;**34**:1224−31.
7. Ericksonmiller CL, Pillarisetti K, Kirchner J, Figueroa DJ, Ottesen LH, Martin A, et al. Low or undetectable TPO receptor expression in malignant tissue and cell lines derived from breast, lung, and ovarian tumors. *BMC Canc* 2012;**12**:405.
8. Kurokawa T, Murata S, Zheng Y, Iwasaki K, Kohno K, Fukunaga K, et al. The eltrombopag antitumor effect on hepatocellular carcinoma. *Int J Oncol* 2015;**47**:1696−702.
9. Roth M, Will B, Simkin G, Narayanagari S, Barreyro L, Bartholdy B, et al. Eltrombopag inhibits the proliferation of leukemia cells *via* reduction of intracellular iron and induction of differentiation. *Blood* 2012;**120**:386−94.
10. Fan XC, Steitz JA. Overexpression of HuR, a nuclear-cytoplasmic shuttling protein, increases the *in vivo* stability of ARE-containing mRNAs. *EMBO J* 1998;**17**:3448−60.
11. Kottaloizou I, Giaginis C, Theocharis S. Clinical significance of HuR expression in human malignancy. *Med Oncol* 2014;**31**:161.
12. Meisner N, Hintersteiner M, Mueller K, Bauer R, Seifert J, Naegeli H, et al. Identification and mechanistic characterization of low-molecular-weight inhibitors for HuR. *Nat Chem Biol* 2007;**3**:508−15.
13. Chae MJ, Sung HY, Kim EH, Lee M, Kwak H, Chae CH, et al. Chemical inhibitors destabilize HuR binding to the AU-rich element of TNF-alpha mRNA. *Exp Mol Med* 2009;**41**:824−31.
14. D'Agostino VG, Adami V, Provenzani A. A novel high throughput biochemical assay to evaluate the HuR protein−RNA complex formation. *PLoS One* 2013;**8**:e72426.
15. Wu XQ, Lan L, Wilson DM, Marquez RT, Tsao WC, Gao P, et al. Identification and validation of novel small molecule disruptors of HuR-mRNA interaction. *ACS Chem Biol* 2015;**10**:1476−84.
16. Manzoni L, Zucal C, Maio DD, Dagostino VG, Thongon N, Bonomo I, et al. Interfering with HuR−RNA interaction: design, synthesis and biological characterization of tanshinone mimics as novel, effective HuR inhibitors. *J Med Chem* 2018;**61**:1483−98.
17. Blanco FF, Preet R, Aguado A, Vishwakarma V, Stevens LE, Vyas A, et al. Impact of HuR inhibition by the small molecule MS-444 on colorectal cancer cell tumorigenesis. *Oncotarget* 2016;**7**:74043−58.
18. Lal P, Cerofolini L, Agostino VGD, Zucal C, Fuccio C, Bonomo I, et al. Regulation of HuR structure and function by dihydrotanshinone-I. *Nucleic Acids Res* 2017;**45**:9514−27.
19. Abdelmohsen K, Gorospe M. Posttranscriptional regulation of cancer traits by HuR. *Wiley Interdiscip Rev RNA* 2010;**1**:214−29.
20. Masoud GN, Li W. HIF-1 alpha pathway: role, regulation and intervention for cancer therapy. *Acta Pharm Sin B* 2015;**5**:378−89.
21. Modi Y, Zhang J, Yarovinsky TO, Rao GK, Collinge M, Zhu Y, et al. Macrophage β2 integrin-mediated, HuR-dependent stabilization of angiogenic factor-encoding mRNAs in inflammatory angiogenesis. *Invest Ophthalmol Vis Sci* 2009;**50**:3755.
22. Chang S, Lu Y, Li X, Hsieh W, Xiong Y, Ghosh M, et al. Antagonistic function of the RNA-binding protein HuR and miR-200b in post-transcriptional regulation of vascular endothelial growth factor-A expression and angiogenesis. *J Biol Chem* 2013;**288**:4908−21.
23. Ke Y, Han Y, Guo X, Wen J, Wang K, Jiang X, et al. PARP1 promotes gene expression at the post-transcriptional level by modulating the RNA-binding protein HuR. *Nat Commun* 2017;**8**:14632.
24. Sui Y, Wu Z. Alternative statistical parameter for high-throughput screening assay quality assessment. *J Biomol Screen* 2007;**12**:229−34.
25. Zhu YY, Huang P, Yang N, Liu R, Liu XT, Dai HQ, et al. Establishment and application of a high throughput screening system targeting the interaction between HCV internal ribosome entry site and human eukaryotic translation initiation factor 3. *Front Microbiol* 2017;**8**:977.
26. Wang H, Zeng F, Liu Q, Liu H, Liu Z, Niu L, et al. The structure of the ARE-binding domains of Hu antigen R (HuR) undergoes conformational changes during RNA binding. *Acta Crystallogr D Biol Crystallogr* 2013;**69**:373−80.
27. Seeliger D, De Groot BL. Ligand docking and binding site analysis with PyMOL and Autodock/Vina. *J Comput Aided Mol Des* 2010;**24**:417−22.
28. Liu BA, Jablonowski K, Shah E, Engelmann BW, Jones RB, Nash PD. SH2 domains recognize contextual peptide sequence information to determine selectivity. *Mol Cell Proteomics* 2010;**9**:2391−404.
29. Zhang Y, Wang ZH, Ma XY, Yang SN, Hu XY, Tao J, et al. Glycyrrhetinic acid binds to the conserved P-loop region and interferes with the interaction of RAS-effector proteins. *Acta Pharm Sin B* 2019;**9**:294−303.
30. Lal S, Cheung E, Zarei M, Preet R, Chand SN, Mambellilisboa NC, et al. CRISPR knockout of the HuR gene causes a xenograft lethal phenotype. *Mol Cancer Res* 2017;**15**:696−707.
31. Lal P, Cerofolini L, D'Agostino VG, Zucal C, Fuccio C, Bonomo I, et al. Regulation of HuR structure and function by dihydrotanshinone-I. *Nucleic Acids Res* 2017;**45**:9514−27.

32. Young LE, Sanduja S, Bemis-Standoli K, Pena EA, Price RL, Dixon DA. The mRNA binding proteins HuR and tristetraprolin regulate cyclooxygenase 2 expression during colon carcinogenesis. *Gastroenterology* 2009;**136**:1669−79.
33. Zhu LF, Li M, Liu XY, Du L, Jin YG. Inhalable oridonin-loaded poly(lactic-*co*-glycolic) acid large porous microparticles for *in situ* treatment of primary non-small cell lung cancer. *Acta Pharm Sin B* 2017;**7**:80−90.
34. Zhang J, Cui Q, Zhao Y, Guo R, Zhan C, Jiang P, et al. Mechanism of angiogenesis promotion with Shexiang Baoxin Pills by regulating function and signaling pathway of endothelial cells through macrophages. *Atheroscler* 2019;**292**:99−111.
35. Dufies M, Giuliano S, Ambrosetti D, Claren A, Ndiaye PD, Mastri M, et al. Sunitinib stimulates expression of VEGFC by tumor cells and promotes lymphangiogenesis in clear cell renal cell carcinomas. *Cancer Res* 2017;**77**:1212−26.
36. Peritz T, Zeng F, Kannanayakal TJ, Kilk K, Eiriksdottir E, Langel U, et al. Immunoprecipitation of mRNA-protein complexes. *Nat Protoc* 2006;**1**:577−80.
37. Kramer N, Walzl A, Unger C, Rosner M, Krupitza G, Hengstschlager M, et al. *In vitro* cell migration and invasion assays. *Mutat Res Rev Mutat Res* 2013;**752**:10−24.
38. Ponce ML. *In vitro* matrigel angiogenesis assays. *Methods Mol Med* 2001;**46**:205−9.
39. Mcgrath JC, Drummond GB, Mclachlan EM, Kilkenny C, Wainwright CL. Guidelines for reporting experiments involving animals: the ARRIVE guidelines. *Br J Pharmacol* 2010;**160**:1573−6.
40. Zucal C, Agostino VGD, Loffredo R, Mantelli B, Natthakan Thongon, Lal P, et al. Targeting the multifaceted HuR protein, benefits and caveats. *Curr Drug Targets* 2015;**16**:499−515.
41. Eberhardt W, Badawi A, Biyanee A, Pfeilschifter J. Cytoskeleton-dependent transport as a potential target for interfering with post-transcriptional HuR mRNA regulons. *Front Pharmacol* 2016;**7**:251.
42. Dagostino VG, Lal P, Mantelli B, Tiedje C, Zucal C, Thongon N, et al. Dihydrotanshinone-I interferes with the RNA-binding activity of HuR affecting its post-transcriptional function. *Sci Rep* 2015;**5**:16478.
43. Wang Z, Bhattacharya A, Ivanov DN. Identification of small-molecule inhibitors of the HuR/RNA interaction using a fluorescence polarization screening assay followed by NMR validation. *PLoS One* 2015;**10**.
44. Griseri P, Pages G. Control of pro-angiogenic cytokine mRNA half-life in cancer: the role of AU-rich elements and associated proteins. *J Interferon Cytokine Res* 2014;**34**:242−54.
45. Xie J, Liu JH, Liu H, Liang SH, Lin MG, Gu YY, et al. The antitumor effect of tanshinone IIA on anti proliferation and decreasing VEGF/VEGFR2 expression on the human non-small cell lung cancer A549 cell line. *Acta Pharm Sin B* 2015;**5**:554−63.
46. Wang H, Li H, Shi H, Liu Y, Liu H, Zhao H, et al. Preliminary crystallographic analysis of the RNA-binding domain of HuR and its poly(U)-binding properties. *Acta Crystallogr F* 2011;**67**:546−50.
47. Albini A, Bruno A, Noonan DM, Mortara L. Contribution to tumor angiogenesis from innate immune cells within the tumor microenvironment: implications for immunotherapy. *Front Immunol* 2018;**9**:527.
48. Qian BZ, Pollard JW. Macrophage diversity enhances tumor progression and metastasis. *Cell* 2010;**141**:39−51.
49. Squadrito ML, de Palma M. Macrophage regulation of tumor angiogenesis: implications for cancer therapy. *Mol Aspect Med* 2011;**32**:123−45.
50. Baer C, Squadrito ML, Iruelaarispe ML, De Palma M. Reciprocal interactions between endothelial cells and macrophages in angiogenic vascular niches. *Exp Cell Res* 2013;**319**:1626−34.